56–62 *Nucleic Acids Research, 2016, Vol. 44, No. 1* *Published online 9 December 2015*
doi: 10.1093/nar/gkv1364

Probing the reactivity of singlet oxygen with purines

Elise Dumont[1,*], Raymond Grüber[1], Emmanuelle Bignon[1,2], Christophe Morell[2], Yohann Moreau[3], Antonio Monari[4,5] and Jean-Luc Ravanat[6,7,*]

[1]Laboratoire de Chimie, UMR 5182, Ecole Normale Supérieure de Lyon, Lyon France, [2]Institut des Sciences Analytiques, Université de Lyon 1 and CNRS, Villeurbanne, France, [3]iRTSV/CBM/MCT, CEA Grenoble, France, [4]Theory-Modeling-Simulation, SRSMC, Université de Lorraine Nancy, Vandoeuvre-lès-Nancy, France, [5]CNRS, Theory-Modeling-Simulation, SRSMC, Vandoeuvre-lès-Nancy, France, [6]INAC-SCIB, Université Grenoble Alpes, F-38000 Grenoble, France and [7]CEA, INAC-SCIB-LAN, F-38000 Grenoble, France

Received August 28, 2015; Revised November 20, 2015; Accepted November 24, 2015

ABSTRACT

The reaction of singlet molecular oxygen with purine DNA bases is investigated by computational means. We support the formation of a transient endoperoxide for guanine and by classical molecular dynamics simulations we demonstrate that the formation of this adduct does not affect the B-helicity. We thus identify the guanine endoperoxide as a key intermediate, confirming a low-temperature nuclear magnetic resonance proof of its existence, and we delineate its degradation pathway, tracing back the preferential formation of 8-oxoguanine versus spiro-derivates in B-DNA. Finally, the latter oxidized 8-oxodGuo product exhibits an almost barrierless reaction profile, and hence is found, coherently with experience, to be much more reactive than guanine itself. On the contrary, in agreement with experimental observations, singlet-oxygen reactivity onto adenine is kinetically blocked by a higher energy transition state.

INTRODUCTION

Singlet molecular oxygen ($^1O_2$) lies among the most deleterious reactive oxygen species (1). Indeed, $^1O_2$ is a common source of damage for many biomolecules: lipid (2), protein (3) and DNA (4,5) which can lead to genomic mutations. The reaction mechanism has been established on prototypical systems (ethylene (6), butadiene and benzene (7,8), thiophene (9)), which mimic lipids. Yet less is known concerning the mechanistic processes of singlet-oxygen-driven DNA damage. Experimentally, it has been shown that reaction of $^1O_2$ with DNA is limited to the guanine nucleobase, with induction of three main products (10), depicted in Figure 1, that have been identified and experimentally characterized over the years (nuclear magnetic resonance (NMR), mass spectrometry…) (11). At the nucleoside level, spironucleosides **6** were found to be mostly produced, together with 4-hydroxy-8-oxo-2′-deoxyguanosine (4-OH-8-oxodGuo **4**) and 8-oxo-7,8-dihydro-2′-deoxyguanosine (12) (8-oxodGuo **8**). In double-stranded DNA and at cellular level (13), 8-oxodGuo was found to be the major product. It has been shown that 8-oxodGuo is more reactive toward singlet oxygen than undamaged nucleoside dGuo **1** (by about 2 order of magnitude) and that spiro-nucleosides could be also generated through secondary oxidation of 8-oxodGuo (14). Thus, rationalizing the mechanism of formation or dGuo decomposition products is a very challenging task. It is supposed that all guanine decomposition products stem from a primary reaction path ($^1O_2$ addition), depicted in Figure 1. Three intermediates can be written down, which can eventually coexist: their relative ratio can be also strongly environment dependent, in the same way the final products are. In order to rationalize the formation of subproducts for which accurate measurements are available, the central question is probably to assess the feasibility of endoperoxide thermal formation. The initiation of $^1O_2$-induced degradation pathway (Figure 1) is the most critical since the so-formed intermediates have a relative short lifetime. Indeed, guanine endoperoxide is commonly accepted as the key intermediate by almost all the different proposed mechanistic pathways even if its isolation and characterization is extremely difficult due to its short lifetime. Interestingly, the endoperoxide has been characterized as the main reaction product of singlet oxygen with aromatic organic compounds, such as anthracene and naphthalene derivatives (15).

Furthermore, and more generally to clarify the reactivity of singlet oxygen toward nucleosides two fundamental questions remain answerless: $^1O_2$ strong selectivity toward guanine versus adenine should be rationalized; the environmentally controlled fragmentation leading to different products between B-DNA and mononucleoside solutions needs to be tackled. To address these questions, in this work, we report computational evidences that unambiguously establish the stability of the guanine endoperoxide **3** *versus* the open zwitterionic intermediate **2-a**, in contrast with previ-

*To whom correspondence should be addressed. Tel: +33 4 72 72 88 46; Email: elise.dumont@ens-lyon.fr
Correspondence may also be addressed to Jean-Luc Ravanat. Tel: +33 38 78 47 97; Email: jean-luc.ravanat@cea.fr

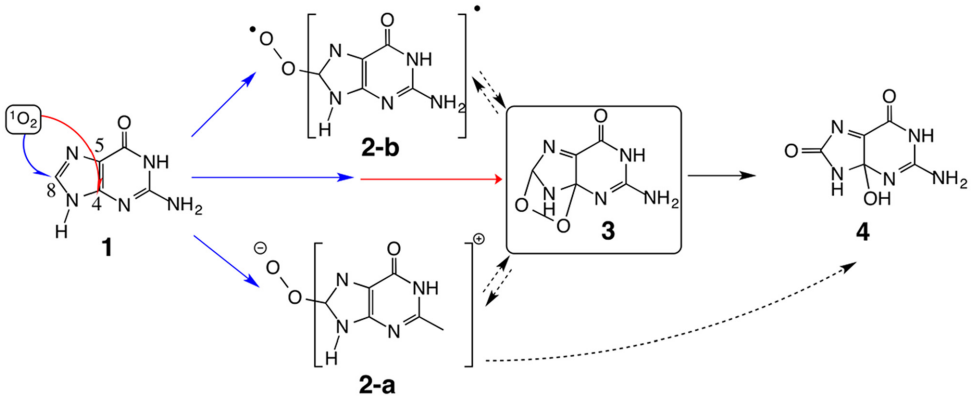

Figure 1. Initial attack of $^1O_2$ onto guanine, up to the endoperoxide intermediate **3**, evolving to the three main experimental products.

ous theoretical approaches (16). We situate an accessible, low-barrier pathway for its formation, which corroborates the existence of a transient guanine endoperoxide. The latter was proposed based on low-temperature NMR experiments performed on a guanosine derivative (17). Within B-DNA, the formation of a cyclic peroxide could eventually trigger an helical distortion energetically penalizing the intermediate **3**.

This hypothesis was tested performing explicit molecular dynamics (MD) simulations of the two intermediates **2-a** and **3** embedded in a 13-bp DNA fragment, and hence excluding any marked structural modifications of the DNA arising from the first attack. Finally, the possible degradation pathways leading respectively to spiro **6** or 8-oxodGuo **8** whether the reaction takes place at the nucleoside level or in B-DNA are explored to assess this environmental effect.

MATERIAL AND METHODS

Quantum mechanics

Quantum mechanics (QM) calculations were conducted starting from a structure of a methyl-capped guanine and a methyl-capped adenine, as a model system, respectively, for 2′-deoxyguanosine and 2′-deoxyadenine. Density functional theory was employed, according to a previous benchmark against the SCS-MP3/aug-cc-pVTZ//MP2/DZP++ (18) level of theory (19) that has stressed out the performance of the range-separated hybrid LC-BLYP. Its performance has been also very recently pinpointed for the singlet-oxygen attack onto trans-resveratrol (20). The Gaussian09 software Revision D.01 (21) was used for all the QM calculations. Since **2** is an intramolecular charge-separated entity and to better model experimental conditions, an implicit model accounting for solvation in water, polarizable continuum model ((22)), was used with a value of the dielectric constant $\epsilon_r = 78.3$. The inclusion of diffuse functions is also important to compare the electronic energies of **2** and **3** on the same footing. We selected the DZP++ basis set, proposed by Schaefer and including diffuse and polarization functions, as a valuable compromise between Pople basis set and the computationally demanding Dunning basis sets. All the stationary points have been characterized by calculating harmonic vibrational forces. Furthermore in the case of transition states intrinsic reaction coordinate profiles have been obtained to assure the transition state (TS) was indeed connecting reactants and products.

Molecular dynamics simulation

All classical MD simulations were performed with the Amber12 Molecular Dynamics software package (23). GAFF (24) and *ff99bsc0* (25) force fields parameters were used. For the oxidized nucleobase, charges and modified force field parameters have been used. Charges were generated using the Restrained Electrostatic Potential charge model of the Antechamber program (26) from QM calculations for the isolated fragment as prescribed by the usual protocol (see Supplementary Table S1): bonded force field parameters along the C-O-O bonds were assigned against high-level QM calculations at the LC-BLYP/DZP++ level of theory. For the open zwitterionic intermediate, the oxygen—oxygen distance is 1.504 Å with a harmonic constant force of 306.30 kcal.mol^{-1}.Å^{-2} (1.42 Å with a force constant of 343.60 kcal.mol^{-1}.Å^{-2} for the endoperoxide). Similarly, the CT…OS linkage for the zwitterionic moiety was taken as 1.439 Å (kr = 301.50 kcal.mol^{-1}.Å^{-2}). For the open structure, the covalent angle C8-O-O was described with an equilibrium value of 103.0 degrees, and an harmonic constant of 65.62 kcal.mol^{-1}.degree^{-2}. For the endoperoxide, the C-O-O angle was assigned to 105.01 degrees with a force constant of 65.89 kcal.mol^{-1}.degree^{-2} (same as c3-os-os in GAFF). The Amber topology input files for the DNA molecule were generated with the LEaP basic preparation program. Endoperoxide and zwitterionic guanine oxidized nucleobases (X) were incorporated into the standard B-DNA conformation of a 13-bp self-complementary alternate poly(dG)-poly(dC) sequence, namely d(GCGCGC**X**CGCGCG):d(CGCGCGCGCGCGC).
For both the endoperoxide and zwitterion intermediates, two different conformations are possible consisting in an attack of ^{1}O2 on guanine either directed toward the 5′ extremity (up) or the 3′ extremity (down). Consequently, a total of four starting structures, endoperoxide up/down and zwitterion up/down, have been built. Negative charges on DNA phosphate groups of each system were neutralized by potassium cations. Modified oligonucleotides with

their counterions were solvated in a 65.4 * 68.4 * 77.3 Å^3 parallelepiped box containing ∼8750 TIP3P water molecules (27) (total ∼27 100 atoms). The Particle Mesh Ewald method with a 9.0 Å cut-off was used for calculation of electrostatic interactions. Throughout the simulation, periodic boundary conditions were employed to eliminate undesirable edge effects. Each system was preliminary minimized in 5000 steps—including 1500 conjugate gradient steps. Heating from the initial temperature of 0–300 K was performed in a thermalization run of 30 ps (NVT ensemble). The temperature was kept constant during MD simulations using the Langevin thermostat (28) with a collision frequency (γ ln) value of 2 ps^{-1}. To ensure an equilibrium sampling, thermalization was followed by an NPT equilibration of 300 ps with pressure of 1 atm., finally a production run of 100 ns was performed for each system. DNA structural parameters were analysed on-the-fly by using the Curves+ code (29); in particular the bending axis and the deviation of inter- and intrastrand parameters from ideal B-DNA's value were considered as an overall measure of the double helix deformation. For a full description of the different base parameters, the reader may refer to the original article by Lavery *et al.* (29). No significant difference concerning DNA distortion or stability is found between up and down conformers. In order to assess the structural stability in more biological relevant conditions MD trajectory for the different conformations were repeated at a temperature of 310 K following the same protocols both for the system set-up and for the analysis of the results.

RESULTS

We first consider the open intermediate **2**, which can a priori exist either as an intramolecular zwitterion **2-a** or as a biradical **2-b**. The energy gap between the two species is in favor of the closed-shell adduct **2-a** in implicit aqueous solvent by 9.2 kcal mol^{-1}: this will be reinforced within B-DNA since the peroxylate –O–O$^-$ moiety is highly solvent exposed (see Supplementary Figure S4). Only the reactivity of the zwitterionic form **2-a** is considered hereafter. Its formation upon nucleophilic attack of $^1O_2$ onto guanine is revealed as an efficient, exothermic process (-10.2 kcal mol^{-1}), with an energy barrier for the first transition state structure $\Delta E^{\dagger(1\rightarrow 2a)}$ estimated to 20.1 kcal mol^{-1} (Figure 2, red solid line) for a distance C8…O of 1.82 Å. Our calculations confirm that the nucleophilic attack occurs on the C8 position, which is the most electrophilic position for guanine (30), in comparison to C4 and C5 (see Supplementary Figure S2). The open intermediate **2-a** coexists as two stable conformers, denoted ≪outer≫ and ≪inner≫ in Figure 3, and differing by the dihedral τ(H8C8OO). A transition state TS2 is located between the two conformers at 8.8 kcal mol^{-1} ($\tau = 111.0°$), although this rotation can be expected to proceed more easily and even be barrierless upon inclusion of dynamic and vibrational effects. The inner conformer of the zwitterion is very prone to evolve toward the endoperoxide **3** via an intramolecular cyclization onto the C4 position of guanine, characterized by a low barrier (2.8 kcal mol^{-1}, Figure 2): the gain in energy accounts for -9.4 kcal mol^{-1}, which corresponds to a charge transfer of 0.4 e between the peroxylate moiety and the guanine nucleobase fragments along the closure.

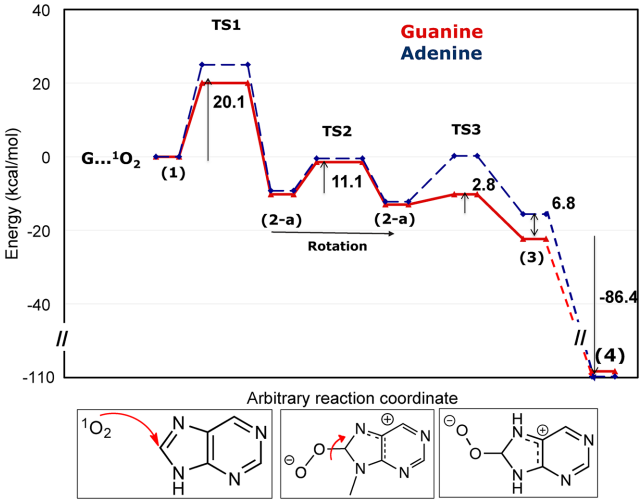

Figure 2. Reaction profile for the purine+$^1O_2$ system (free nucleosides).

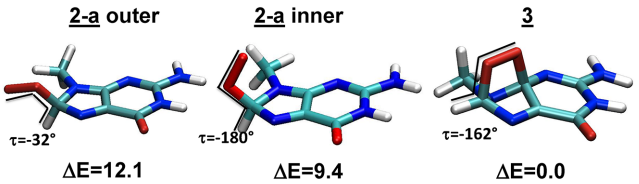

Figure 3. Representation of the guanine+$^1O_2$ intermediates.

To sum up, going from **1** to **3**, the G+$^1O_2$ damaging process is driven by a considerable thermodynamic force, the endoperoxide **3** being -22.4 kcal mol^{-1} more stable than the {G+$^1O_2$} adduct in its equilibrium geometry (at a distance $^1O_2$…C8 of 2.59 Å). The addition onto C8 clearly stands out as the limiting step. The existence of a second possible channel, the synchronous process with the [4+2] cycloaddition of $^1O_2$ across the 4,8-bond of the imidazole ring, leading to **3** directly from **1** (Figure 1) cannot be assessed due to its multireference character (7). But in case of a low barrier, this channel would reinforce our statement surmising the guanine endoperoxide as a key intermediate in guanine oxidation pathway as depicted in Figure 2.

The low ionization potential of guanine comes to stabilize the intramolecular adduct **2-a**, as revealed by comparison with the adenine profile: however the main difference for the profiles of the two bases is a higher transition state for the initial attack onto adenine ($\Delta E^{\dagger(1\rightarrow 2)} = 25.0$ kcal mol^{-1}, Figure 2 blue dashed line). The propensity to stabilize a partial positive charge on the guanine ring constitutes an additional driving force towards its oxidation. The selectivity of reaction of $^1O_2$ toward DNA constituents can therefore be explained on the basis of a kinetic blockage hampering the formation of the endoperoxide for adenine and more specifically the C8 addition. It is also noticeable that the critical O…C8 distance for adenine is found to be significantly lower (1.76 Å). Another feature is the less pronounced stability of the adenine endoperoxide structure ($\Delta\Delta E = 6.8$ kcal mol^{-1}), due to electronic factors since no difference of

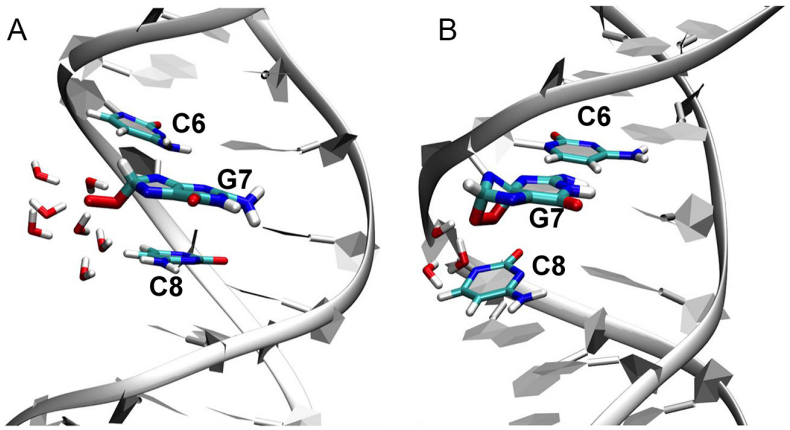

Figure 4. Representative structures for guanine intermediates **2-a** and **3**. Water molecules within 5 Å of O_2 are depicted.

geometries is predicted. Our interpretation is reinforced as no such energy difference is found for all the other intermediates that are planar. Also the closure of the endoperoxide is found to be more difficult with adenine ($TS^{(2\rightarrow3)}$ with a barrier of 10.5 kcal mol^{-1}) probably again due to a more strained structure. Globally these results put on a firm basis the existence of a kinetic blockage. We also note that the charge-separated intermediate **2-a** will be further stabilized by a 3′-purine, as known experimentally for reactions implying electron transfer, by ∼1 kcal mol^{-1} according to auxiliary calculations (Supplementary Figure S4).

The energetic profile in Figure 2 may differ as the singlet-oxygen reaction profile is considered for guanine embedded within a ds-DNA fragment. In particular large deformation of the DNA induced by the guanine oxidation could impose strong additional deformation-free energy, while the mechanical constrains could be seen as further factors producing potential kinetic blockages. To assess DNA structural stability, explicit-solvent MD were performed for an alternate poly(dG)-poly(dC)13-bp sequence where the seventh nucleobase is an oxidized guanine. Such simulations allow us to probe the local environment experienced by **2-a** or **3**, which can tune the relative energies. In turn, our simulations palliate the absence of experimental structures for these high-lying intermediates. The non-planar structure may jeopardize the endoperoxide stability within B-DNA by disrupting π-stacking with adjacent nucleobases C6 and C8 and possibly the Watson-Crick pairing with cytosine C20 on the representative 13-bp sequence depicted in Figure 4, weakening the three canonical hydrogen bonds. The global structural stability of the DNA double helix even in presence of the zwitterionic or endoperoxide intermediates is confirmed by the structural analysis performed along the MD trajectory. Indeed, the bending of the helix is quite modest assuming an average value of 13±6° at 300 K and of 20±10° at 310 K (Figure 5). Also the inter- and intrabasis parameters do not show any significant deviation from the ideal B-DNA values, and most notably the deviation from ideality experienced by the oxidized base-pair remains shy compared to the adjacent base-pair. The opening parameter is modest while a shift of 2 Å concomitant to a combined roll and tilt of ca. 15° are the most noticeable feature. However, those deformations are not accompanied by other significant intrastrand deviation (Supplementary Figure S5a). The same picture holds also for the higher temperature dynamics (see Supplementary Figure S5b). Such deformations are also small when compared to other DNA defects such as photodimers (31) and oxidative intrastrand cross-links (32). Besides G7, C6 is the most impacted nucleobase of the oligonucleotide, with a high 'stagger' to prevent a steric clash with the peroxo bridge. The zwitterionic intermediate is even more structurally innocent on the B-helicity (see Supplementary Figure S6). Hence, we can conclude that even if some strains are present, those differences are quite local and are not indicative of a strong enough structural deformation to preclude the embedding of the endoperoxide or zwitterion intermediates. We note that the solvation pattern and the main B-helical characteristic remain similar upon increase of the temperature to 310 K (see Supplementary Figure S7). Indeed apart from an increased thermal fluctuation, notably leading to a slightly larger bending, all the other main structural parameters are almost unaltered upon increase of the temperature.

From this analysis we conclude that no significant mechanical strain or deformation is induced on DNA structure by the oxidation, confirming the high probability of the existence of such intermediates. Note that as previously cited in the case of **2-a**, the terminal oxygen atom is strongly solvent exposed and hence the zwitterionic form is still favored compared to the diradical (see Supplementary Figure S3).

Downhill, our calculations confirm the experimental fact that the degradation cascade which starts from the endoperoxide **3** is most likely to continue the 4-hydroxy-8-oxo-2′-deoxyguanosine **4**. Stabilization energy accounts for 86.4 kcal mol^{-1} (Figure 2), a considerable exothermicity due to a release of the conformational strain of the endoperoxide (33), reflected in the lenghtening of the C8-O1 bond from 1.35 to 1.44 Å, and an increase of conjugation along the π-system. The rate-limiting step is found to be the opening of the endoperoxide (Figure 6) that implies a high-energy transition state situated at ca. 44 kcal mol^{-1} with at least two water molecules. The latter provides a shuttle for the proton transfer and eventually contributes to stabilize the partially negatively charged oxygen O_2 (see Supplementary Table S1). This channel can occur for solvated guanine ow-

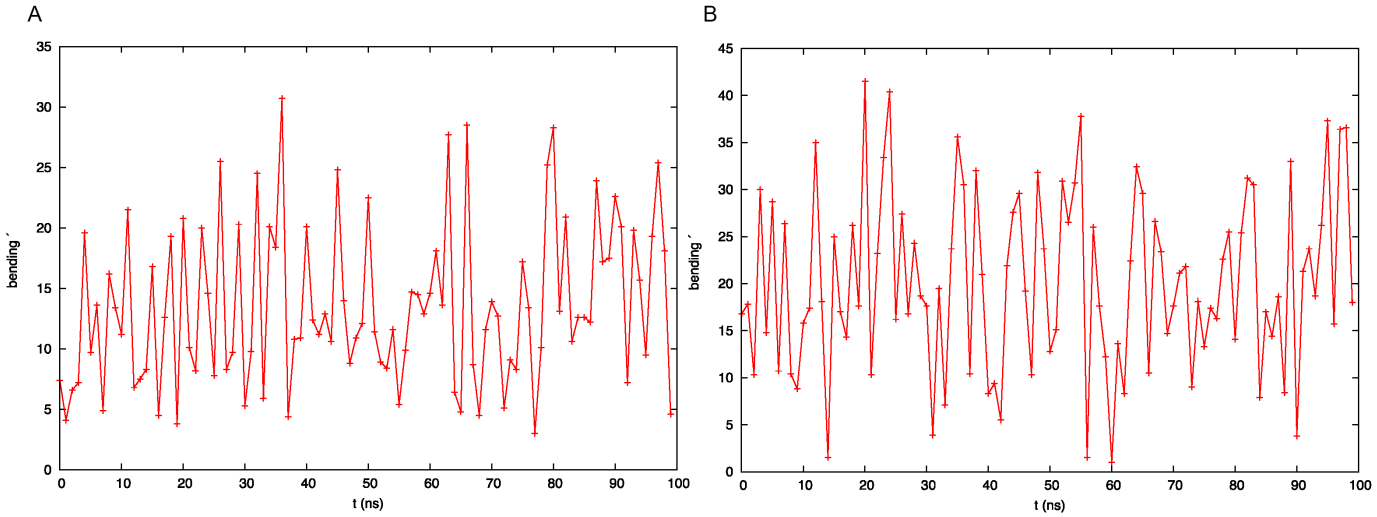

Figure 5. Evolution of the DNA double-strand axis bending all along the MD trajectory for the zwitterion (a) and the endoperoxide (b), respectively.

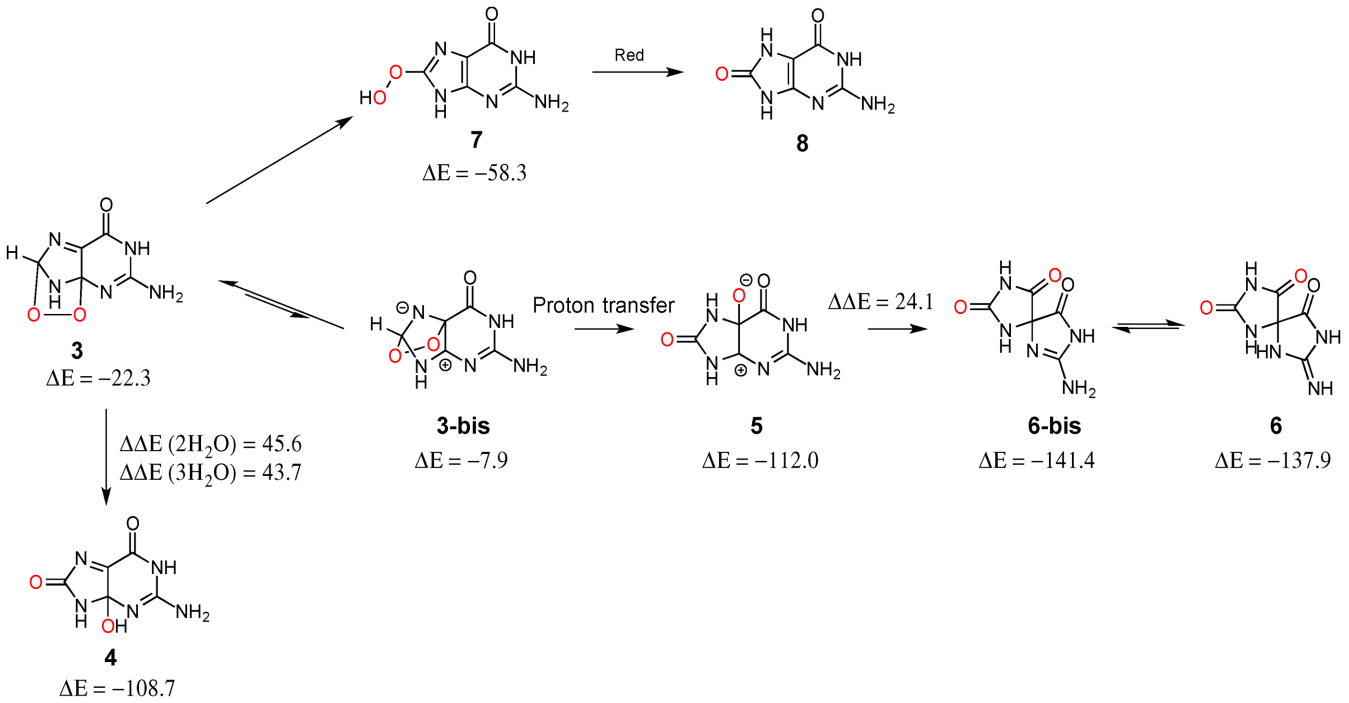

Figure 6. Relative energies (in kcal mol^{-1}) corresponding to three decomposition schemes for the endoperoxide **3**.

ing to dynamic effects that would further lower the barrier. The presence of a chemical species acting as a base would also assist the endoperoxide opening via a Kornblum-De Le Mare reaction (34). Another possible evolution of the endoperoxide **3** (Figure 6) will lead to the formation of the spironucleoside **6**, for which we identified a plausible reaction path via the migration of the oxygen O_2 onto the C5 position of the guanine ring, followed by a proton transfer. This last step constitutes the driving force with an energetic stabilization of -104.1 kcal mol^{-1}. Finally, it has been proposed that 8-oxodGuo can also further react with $^1O_2$ and undergo singlet-oxygen addition onto the C4 = C5 ethylenic bond (the C8 position is no longer available). We have computed the transition state structure for the attack of $^1O_2$ onto C4 position of the oxidized nucleobase and the barrier has been estimated to be lower than 2 kcal mol^{-1} (see ESI). This very small barrier is totally consistent with the experimental report of a 100-fold higher reactivity compared to guanine.

DISCUSSION

The oxidative attack of $^1O_2$ onto guanine has been rationalized both from a kinetic and an energetic points of view based on combined high-level quantum chemistry calculations and MD simulations. In particular mechanistic hy-

potheses explaining the peculiarity of this reaction have been presented. We report strong evidences for the singlet-oxygen attack onto guanine to proceed in two steps to yield an endoperoxide, via an open zwitterionic intermediate. Activation energies compatible with a thermally allowed reaction have been obtained in the case of guanine. The selectivity of $^1O_2$ for guanine compared to adenine has been rationalized too, as the attack on the guanine ring proceeds via lower activation energies, and leads to larger driving forces. On the other hand, the attack of singlet oxygen to 8-oxodGuo has been found to have only a very negligible barrier, rationalizing the experimentally observed larger reactivity than guanine itself. MD simulations, at room and body characteristic temperature, have also confirmed that B-DNA accommodates both endoperoxide and zwitterionic intermediates with no marked distortion. This observation is consistent with the fact that the endoperoxide has been isolated at low temperature, and strongly confirms its crucial role in determining DNA oxidation. For this first part of the singlet-oxygen attack, it would be desirable to further probe this reactivity within an explicitly solvated oligonucleotide, including the temperature and electrostatic embedding of a B-helix, resorting to hybrid quantum mechanics/molecular mechanics to evaluate free energies of activation. However, even if our isolated model for the reactivity is much simpler, we are confident that the same mechanistic picture will hold, even if the exact amount of the kinetic barrier could change. Hence, despite the limitations due to the simplified treatment of the environment, our computational scheme provides a chemically sound explanation of an ubiquitous reaction.

We modeled the strongly exoergonic further degradation of endoperoxide, which implies more complex reaction coordinates and the assistance of two water molecules probed along the classical MD trajectories. Indeed with this assistance endoperoxide can initiate a reactive cascade leading to spiro product, which happens to be the main reaction product in water solution. On the contrary in DNA this path is kinetically blocked, since MD proved water molecules can rarely reach the endoperoxide and the proximal phosphate group disfavors the occurrence of partially negatively-charged intermediates. The water-shielding effect of DNA helix was confirmed both for the 300 and 310 MD trajectories. Instead, an alternative degradation pattern is initiated that goes toward endoperoxide and subsequent fast production of 8-oxodGuo. Hence, the DNA tuning of reactivity has been rationalized and confirmed.

SUPPLEMENTARY DATA

Supplementary Data are available at NAR Online.

ACKNOWLEDGEMENTS

The Pole de Simulation Numérique et Modélisation (PSMN) is acknowledged for the computational resources. E.B. is grateful for a Ph.D. fellowship from the French Minister of Higher Education and Research.

FUNDING

COST action in Chemistry Action CM 1201 'Biomimetic Radical Chemistry'; Labex PRIMES [ANR-11-LABX-0063]. Funding for open access charge: Labex PRIMES [ANR-11-LABX-0063].
Conflict of interest statement. None declared.

REFERENCES

1. Triantaphylidès,C., Krischke,M., Hoeberichts,F.A., Ksas,B., Gresser,G., Havaux,M., Van Breusegem,F. and Mueller,M. J. (2008) Environmental stress and adaptation to stress. *Plant Phys.*, **148**, 960–968.
2. Stratton,S.P. and Liebler,D.C. (1997) Determination of singlet oxygen-specific versus radical-mediated lipid peroxidation in photosensitized oxidation of lipid bilayers: effect of β-Carotene and α-tocopherol. *Biochemistry*, **36**, 12911–12920.
3. Davies,M.J. (2003) Singlet oxygen-mediated damage to proteins and its consequences. *Biochem. Biophys. Res. Comm.*, **305**, 761–770.
4. Devasagayam,T.P.A., Steenken,S., Obendorf,M.S.W., Schulz,W.A. and Sies,H. (1991) Formation of 8-hydroxy(deoxy)guanosine and generation of strand breaks at guanine residues in DNA by singlet oxygen. *Biochemistry*, **30**, 6283–6289.
5. Piette,J. (1991) New trends in photobiology: biological consequences associated with DNA oxidation mediated by singlet oxygen. *J. Photochem. Photobiol. B*, **11**, 241–260.
6. Saito,T., Nishihara,S., Kataoka,Y., Nakanishi,Y., Kitagawa,Y., Kawakami,T., Yamanaka,S., Okumura,M. and Yamaguchi,K. (2010) Reinvestigation of the reaction of ethylene and singlet oxygen by the approximate spin projection method. Comparison with multireference coupled-cluster calculations. *J. Phys. Chem. A*, **114**, 7967–7974.
7. Bobrowski,M., Liwo,A., Oldziej,S., Jeziorek,D. and Ossowski,T. (2000) CAS MCSCF/CAS MCQDPT2 study of the mechanism of singlet oxygen ddition to 1, 3-butadiene d benzene. *J. Am. Chem. Soc.*, **122**, 8112–8119.
8. Leach,A.G. and Houk,K.N. (2002) Diels-Alder and ene reaction of singlet oxygen, nitroso compounds and triazolinediones: transition states and mechanism from contemporary theory. *Chem. Commun.*, **12**, 1243–1255.
9. Song,X., Fanelli,M.G., Cook,J.M., Bai,F. and Parish,C.A. (2012) Mechanism for the reaction of thiophene and methylthiophene with singlet and triplet molecular oxygen. *J. Phys. Chem. A*, **116**, 4934–4946.
10. Ravanat,J.-L. and Cadet,J. (1995) Reaction of singlet oxygen with 2′-deoxyguanosine and DNA. Isolation and characterization of the main oxidation products. *Chem. Res. Toxicol.*, **8**, 379–388.
11. Cadet,J., Ravanat,J.-L., Martinez,G., Medeiros,M. and Di Mascio,P. (2006) Singlet oxygen oxidation of isolated and cellular DNA: product formation and mechanistic insights. *Photochem. Photobiol.*, **82**, 1219–1225
12. Ravanat,J.-L., Martinez,G.R., Medeiros,M.H., Di Mascio,P. and Cadet,J. (2006) Singlet oxygen oxidation of 2′-deoxyguanosine. Formation and mechanistic insights. *Tetrahedron*, **62**, 10709–10715.
13. Ravanat,J.-L., Di Mascio,P., Martinez,G.R., Medeiros,M.H.G. and Cadet,J. (2000) Singlet oxygen induces oxidation of cellular DNA. *J. Biol. Chem.*, **275**, 40601–40604.
14. Martinez,G.R., Medeiros,M.H.G., Ravanat,J.-L., Cadet,J. and Di Mascio,P. (2002) 18O-labeled singlet oxygen as a tool or mechanistic studies of 8-oxo-7, 8-dihydroguanine oxidative damage: detection of spiroiminodihydantoin, imidazolone, and oxazolonederivatives. *Biol. Chem.*, **383**, 607–617.
15. Martinez,G.R., Ravanat,J.-L., Medeiros,M.H.G., Cadet,J. and Di Mascio,P. (2000) Synthesis of a naphthalene endoperoxide as a source of 18O-labeled singlet oxygen for mechanistic studies. *J. Am. Chem. Soc.*, **122**, 10212–10213.
16. Sheu,C. and Foote,C.S. (1993) Endoperoxide formation in guanosine derivatives. *J. Am. Chem. Soc.*, **115**, 10446–10447.
17. Kushwaha,P.S. and Mishra,P.C. (2005) Binding of singlet oxygen with a stacked guanine dimer. *Int. J. Quant. Chem.*, **102**, 435–442.

18. Gu,J., Wang,J. and Leszczynski,J. (2010) Electron attachment-induced DNA single-strand breaks at the pyrimidine sites. *Nucleic Acids Res.*, **38**, 5280–5290.
19. Grüber,R., Monari,A. and Dumont,E. (2014) Stability of the guanine endoperoxide intermediate: a computational challenge for density functional theory. *J. Phys. Chem. A*, **118**, 11612–11619.
20. Mazzone,G., Alberto,M.E., Russo,N. and Sicilai,E. (2014) Ab-initio calculation of the $^1O_2$ quenching mechanism by trans-resveratrol. *Phys. Chem. Chem. Phys.*, **16**, 12773–12781.
21. Frisch,M.J., Trucks,G.W., Schlegel,H.B., Scuseria,G.E., Robb,M.A., Cheeseman,J.R., Scalmani,G., Barone,V., Mennucci,B., Petersson,G.A. *et al.* (2009) *Gaussian09 Revision D.01*. Gaussian Inc., Wallingford C.
22. Tomasi,J., Mennucci,B. and Cammi,R. (2005) Quantum mechanical continuum solvation models. *Chem. Rev.*, **105**, 2999–3094.
23. Case,D.A., Berryman,J.T., Betz,R.M., Cerutti,D.S., Cheatham,T.E. III, Darden,T.A., Duke,R.E., Giese,T.J., Gohlke,H., Goetz,A.W. *et al.* (2015) *AMBER 2015*, University of California, San Francisco.
24. Wang,J., Wolf,R.M., Caldwell,J.W., Kollman,P.A. and Case,D.A. (2004) Developing and testing a general amber force field. *J. Comp. Chem.*, **25**, 1157–1174.
25. Pérez,A., Marchan,I., Svozil,D., Sponer,J., Cheatham,T.E. III, Laughton,C.A. and Orozco,M. (2007) Refinement of the Amber force field for nucleic acids: improving the description of α/γ conformers. *Biophys. J.*, **92**, 3817–3829.
26. Cieplak,P., Cornell,W.D., Bayly,C. and Kollman,P.A. (1995) Application of the multimolecule and multiconformational RESP methodology to biopolymers: charge derivation for DNA, RNA and proteins. *J. Comp. Chem.*, **16**, 1357–1377.
27. Jorgensen,W.L., Chandraeskar,J., Madura,J.D., Impey,R.W. and Klein,M.L. (1983) Comparison of simple potential functions for simulating liquid water. *J. Chem. Phys.*, **79**, 926–935.
28. Izaguirre,J.A., Catarello,D.P., Wozniak,J.M. and Skeel,R.D. (2001) Langevin stabilization of molecular dynamics. *J. Chem. Phys.*, **114**, 2090–2098.
29. Lavery,R., Moakher,M., Maddocks,J.H., Petkeviciute,D. and Zakrewska,K. (2009) Conformational analysis of nucleic acids revised: curves+. *Nucleic Acids Res.*, **37**, 5917–5929
30. Jena,N.R. (2012) DNA damage by reactive species: mechanism, mutation and repair. *J. Biosci.*, **37**, 503–517.
31. Park,H., Zhang,K., Ren,Y., Nadji,S., Singa,N., Taylor,J.-S. and Kang,C. (2002) Crystal structure of a DNA decamer containing a *cis-syn* thymine dimer. *Proc. Natl. Acad. Sci. U.S.A.*, **99**, 15965–15970
32. Garrec,J., Patel,C., Rothlisberger,U. and Dumont,E. (2012) Insights into intrastrand cross-link lesions of DNA from QM/MM molecular dynamics simulations. *J. Am. Chem. Soc.*, **134**, 2111–2119.
33. Castillo,A. and Greer,A. (2009) Theoretical studies of a singlet oxygen-releasing dioxapaddlane (1, 4-diicosanaphtalene-1, 4-endoperoxide). *Struct. Chem.*, **20**, 399–407.
34. Staben,S.T., Linghu,X. and Toste,F.D. (2006) Enantioselective synthesis of γ-hydroxyenones by chiral base-catalyzed Kornblum DeLaMare rearrangement. *J. Am. Chem. Soc.*, **128**, 12658–12569.